Nanoscale Advances

Accepted Manuscript

This article can be cited before page numbers have been issued, to do this please use: T. Oshikiri, T. Kawase, K. Sato, H. Ito, T. Tomai, K. Nakamura, X. Shi, Y. Matsuo, H. Niinomi and M. Nakagawa, *Nanoscale Adv.*, 2026, DOI: 10.1039/D6NA00165C.

ROYAL SOCIETY OF CHEMISTRY

rsc.li/nanoscale-advances

Photoelectrochemically Homogeneous Nickel Oxide Photocathode Composed of Nanocrystals Prepared by Supercritical Hydrothermal Synthesis

View Article Online
DOI: 10.1039/D6NA00165C

Received 00th January 20xx,
Accepted 00th January 20xx

DOI: 10.1039/x0xx00000x

Tomoya Oshikiri [*,†,a,b], Tomoki Kawase[†,a], Kaori Sato[c], Hazuki Ito[a], Takaaki Tomai[a,d], Keisuke Nakamura[e], Xu Shi[e,f], Yasutaka Matsuo[f], Hiromasa Niinomi[a,b,‡], Masaru Nakagawa[*,a,b]

This study presents a novel approach for fabricating photoelectrochemically homogeneous photocathodes composed of nickel oxide nanocrystals (NiO NCs) using supercritical hydrothermal synthesis and push coating (PC) methods. NiO NCs were synthesized in supercritical water using oleic acid (OA) as a surface modifier. The NiO NCs exhibited high crystallinity, small particle size, and narrow size distribution. Compared with the Langmuir–Schaefer method, the PC method provided NiO-NC films with relatively low roughness and high photoelectrochemical performance. In the PC method, NiO-NC films with thicknesses of ~100–500 nm were obtained by varying the NiO-NC and OA concentrations in the dispersions. The NiO-NC films can be regarded as photoelectrochemically homogeneous photocathodes, as their impedances are proportional to their thicknesses. This homogeneity, in turn, increases the design freedom of NiO photocathodes. In addition, atomic layer deposition allowed the filling of interparticle voids with NiO, improving the hole migration capability of the NiO-NC films. These findings demonstrate the potential of combining supercritical synthesis and PC methods as a green and economically advantageous process for the high-throughput manufacturing of NiO photocathodes, minimizing material loss and limiting the use of hazardous solvents.

Introduction

Wide-bandgap photocathodes, such as cobalt oxide,[1] copper oxide,[2] vanadium oxide,[3] gallium nitride,[4] and copper thiocyanate,[5] have been widely employed in various applications, including visible-light-transmitting conductive layers[6, 7] and hole transport layers in photoelectric conversion[8-12] and sensing devices.[13-15] In particular, nickel oxide (NiO) represents a promising photocathode material owing to its negative conduction band minimum, which enables strong reduction ability and high stability.[16-18] Efficient charge separation and directed carrier migration are critical factors governing the performance of semiconductor systems for photoelectrochemical reaction, and defect states and interfacial charge-transfer pathways strongly influence their efficiency.[19-22]

Our group recently reported a sol–gel process to produce thin films containing crystalline NiO_x particles. Their immersion in a NiO precursor solution and subsequent sintering achieved a high photocathode performance through effective connection of the NiO particles.[23] These findings suggest that increased NiO crystallinity and a reduced number of interparticle voids play key roles in enhancing hole migration in NiO photocathodes. In particular, a high productive method for improving NiO crystallinity is essential in practical photocathode applications. Various procedures have been employed to prepare high-quality NiO films, including evaporation,[24] sputtering,[25] and atomic layer deposition.[26] Additionally, our group previously reported that pulse laser deposition provides thin films of highly crystalline and oriented NiO via epitaxial growth.[27, 28] These NiO thin films function as high-performance photocathodes under modal coupling conditions between localized surface plasmons and Fabry–Pérot nanocavity modes.[29] For practical metal oxide fabrication, solution-phase syntheses are advantageous due to their high throughput and scalability.[30] Besides the aforementioned sol–gel process,[16] hydrothermal and solvothermal syntheses[31, 32] as well as thermal decomposition of organometallic precursors[33, 34] have been reported for preparing highly crystalline metal oxide particles for NiO films. Although particle size distribution is critical in the fabrication of dense and compact films composed of closely packed particles, particle size control remains challenging at the nanometer scale.

Supercritical hydrothermal synthesis, which proceeds in a thermodynamic state above the critical temperature and pressure of water, enables the formation of nanocrystals (NCs) with narrow size distributions and high crystallinity, due to accelerated hydrothermal reactions and subsequent highly supersaturated nucleation.[35-38] Furthermore, supercritical hydrothermal synthesis enables surface modification of NCs with organic molecules during particle formation, which can regulate NC growth and enhance dispersibility in organic solvents. Importantly, the use of supercritical water as a green solvent allows efficient synthesis of metal oxide NCs without the requirement for volatile organic solvents.

Spin-coating of NC dispersions is widely employed to prepare NC films; however, this method suffers from considerable material loss during the initial spinning process,

[a.] *Institute of Multidisciplinary Research for Advanced Materials, Tohoku University, 2-2-1 Katahira, Aoba-ku, Sendai, Miyagi 980-8577, Japan.*
[b.] *Semiconductor Creativity Hub, Tohoku University, Sendai, Miyagi 980-8579, Japan*
[c.] *Institute for Materials Research, Tohoku University, Sendai, Miyagi 980-8577, Japan*
[d.] *Frontier Research Institute for Interdisciplinary Sciences, Tohoku University, 6-6-10 Aramaki, Aoba-ku, Sendai, Miyagi 980-8577, Japan.*
[e.] *Creative Research Institution, Hokkaido University, N20W10, Kita-ku, Sapporo, Hokkaido 001–0021, Japan*
[f.] *Research Institute for Electronic Science, Hokkaido University, N20W10, Kita-ku, Sapporo, Hokkaido 001-0021, Japan*
† These authors contributed equally to this work.
‡ Present address: *WPI-SKCM2, Hiroshima University, Higashhiroshima, Hiroshima, 739-8531, Japan*
Supplementary Information available: [details of any supplementary information available should be included here]. See DOI: 10.1039/x0xx00000x

and the convection during solvent evaporation can lead to inhomogeneous film thickness.[39, 40] The Langmuir–Blodgett and Langmuir–Schaffer (LS) methods have been used to produce compact and homogeneous nanoparticle films.[41, 42] In these techniques, NCs are compressed and assembled at the air–water interface, and the resulting NC films are deposited onto solid surfaces. However, these methods are sensitive to the surface conditions of both the particles and the substrates, including the chemical properties of surface modifiers and the physical roughness of the surface. As a result, the optimal combination of nanoparticles and their substrates is often limited, and the large-area manufacturing of nanoparticle films remains challenging. Recently, the push-coating (PC) method was demonstrated as an effective approach for producing thin films of polymers and organic molecules.[43-45] In this method, a solution is confined within a narrow space between the substrate and a plate, and the solvent is extracted via capillary-driven wetting. This produces flat films while reducing the use of hazardous organic solvents and nanoparticles. The restricted space between the substrate and the plate surfaces, combined with reduced solvent convection, ultimately minimize variations in film thickness. Considering these insights, a novel fabrication method is proposed for NiO-NC films. Initially, the crystallinity, particle size, and NiO-NC distribution are controlled through supercritical hydrothermal synthesis with *in-situ* surface modification. Subsequently, the film formation capability of NiO NCs is investigated through comparison of the LS and PC methods, with a focus on green processing and reduced chemical waste. Moreover, the photocathode performance of the NiO-NC films is evaluated using photoelectrochemical methods.

Results and discussion

Supercritical hydrothermal synthesis and characterization of the NiO NCs

NiO NCs were synthesized via supercritical hydrothermal synthesis, both in the absence and presence of OA (Figure 1a). OA is an aliphatic carboxylic acid with an unsaturated bond that enhances the dispersibility of NCs by reducing interparticle interactions.[46] Initially, nickel nitrate, the NiO precursor, was dissolved in water to form an aqueous Ni^{2+} solution. For the reactions incorporating OA, the aqueous phase separated from the organic OA phase under non-supercritical conditions. The reactor temperature was then increased to 400°C (673 K), at which point the internal pressure was estimated to reach 38 MPa, exceeding the critical temperature (646 K) and pressure (22.1 MPa) of water, thus achieving supercritical conditions.[38] Under these conditions, NiO NCs nucleated from the supersaturated aqueous phase, while OA mixed with the supercritical water due to its low dielectric constant. Subsequently, the system was cooled to quench the reaction. The organic and aqueous phases were separated again, giving OA-modified NiO NCs dispersed in the organic phase.

Figures 1b and 1c show the transmission electron microscope (TEM) images of the NiO NCs. The NiO NCs prepared in the absence of OA exhibited various polymorphisms and a large particle size distribution, with a maximum particle diameter of ~200 nm. In contrast, the NiO NCs prepared in the presence of OA exhibited an isotropic shape with diameters of 10–20 nm. Figure 1d shows the X-ray diffraction (XRD) patterns of the NiO NCs after a reaction time of 20 min. The NCs prepared in both the absence and presence of OA exhibited clear diffraction peaks derived from NiO. Diffraction peaks derived from other byproducts, such as nickel hydroxide, were not observed, indicating that the supercritical hydrothermal reaction rapidly generated NiO, consistent with previous reports.[37] The Fourier-transform infrared (FTIR) spectrum of the NiO NCs prepared in the presence of OA showed vibrational signals derived from symmetric and asymmetric -CH_2 stretches at 2800–3000 cm^{-1}, and from the symmetric and asymmetric -COO^- stretches at 1400–1600 cm^{-1} (Figure 1e).[47] These signals were not observed in the spectrum of the NiO NCs prepared in the absence of OA, confirming successful modification of the NiO NCs with OA after synthesis and purification.

The NiO NCs prepared by supercritical hydrothermal synthesis in the presence of OA exhibited small particle diameters and high crystallinity, and the particle surfaces were modified with OA. These characteristics are favorable for producing compact photocathode films from NiO NC dispersions.

NiO-NC film fabrication using the PC method

A flat poly(dimethylsiloxane) (PDMS) film was used as a mold to absorb the hydrophobic solvent. Specifically, a droplet of a 3 wt% NiO NC dispersion in *n*-octane was placed on a glass substrate coated with a transparent, electrically conductive film with high thermal durability (TEC glass) and compressed using the PDMS mold, as shown in Figure 2a. The TEC layer with a thickness of approximately 250 nm was possibly composed of indium tin oxide and tin oxide and employed to transport holes from NiO-NC film to the electrochemical apparatus. For comparison, NiO-NC films were also prepared using the LS method. In both cases, the organic reagents were removed from the films by annealing and ultraviolet (UV)/O_3 treatment after film coating, as confirmed by FTIR spectroscopy of the resulting NiO NCs (Figure S1). The top-view image of NiO-NC film observed by field-emission scanning electron microscopy (FE-SEM) in Figure 2b shows that aggregated secondary particles of NiO NCs with submicro- to micrometer sizes were deposited on the substrate by the LS method. In contrast, for the PC method, the secondary particles measured several tens of nanometers in size (Figure 2c). Based on the SEM images, the coverage ratios (CRs) of NiO-NCs on the TEC glass substrates were calculated (Table 1). Table 1 also provides the average thicknesses and surface roughnesses of the NiO-NC films, which were determined from the height profiles shown in Figures S2a and S2b. The roughness of the NiO-NC film prepared using the LS method was 90 nm, which is >2–3-fold larger than that of the

View Article Online
DOI: 10.1039/D6NA00165C

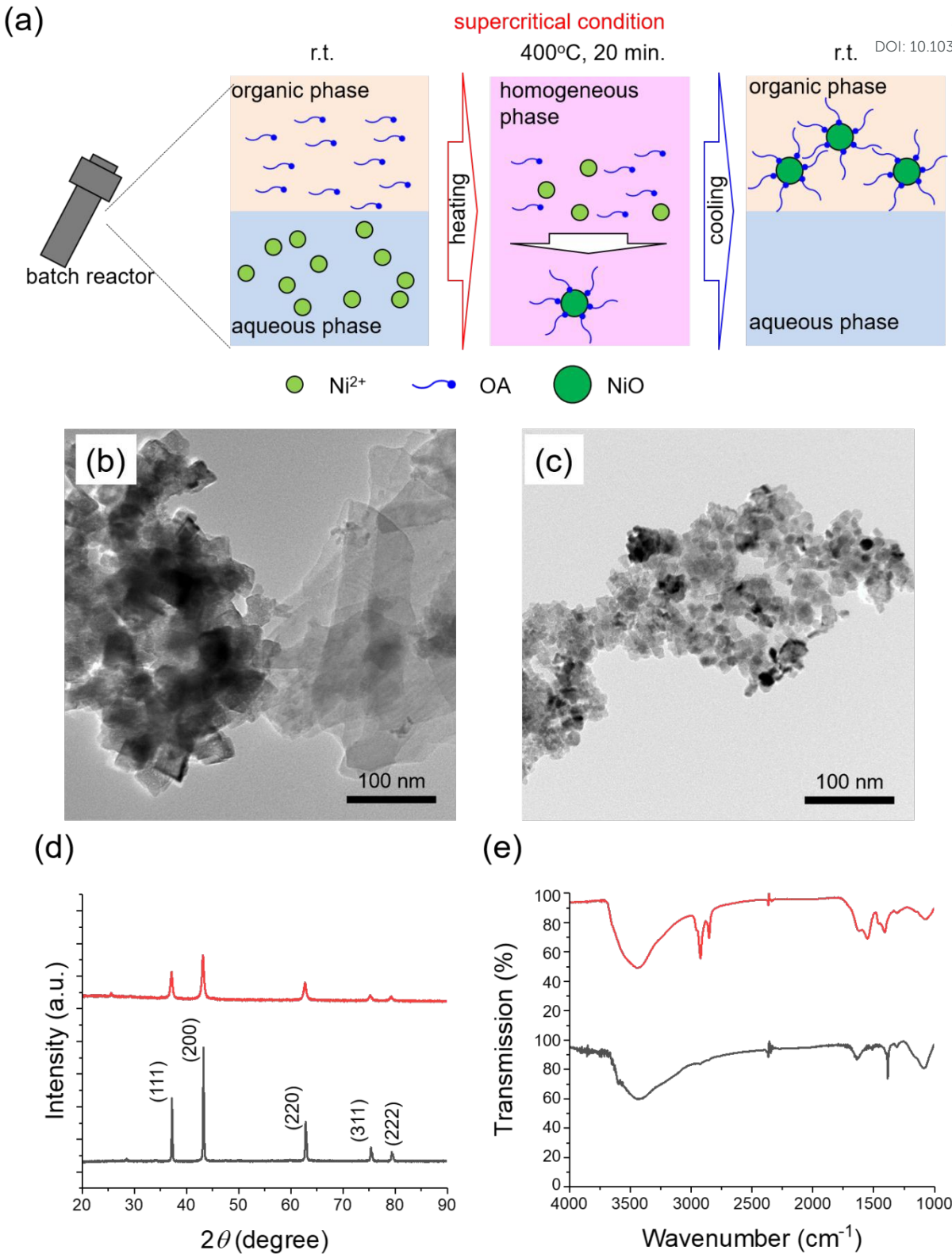

Fig. 1 (a) Schematic illustration of the supercritical synthesis of the NiO NCs. TEM images of the NiO NCs prepared in the (b) absence and (c) presence of OA. (d) XRD patterns and (e) IR spectra of the NiO NCs prepared in the (black) absence and (red) presence of OA.

View Article Online
DOI: 10.1039/D6NA00165C

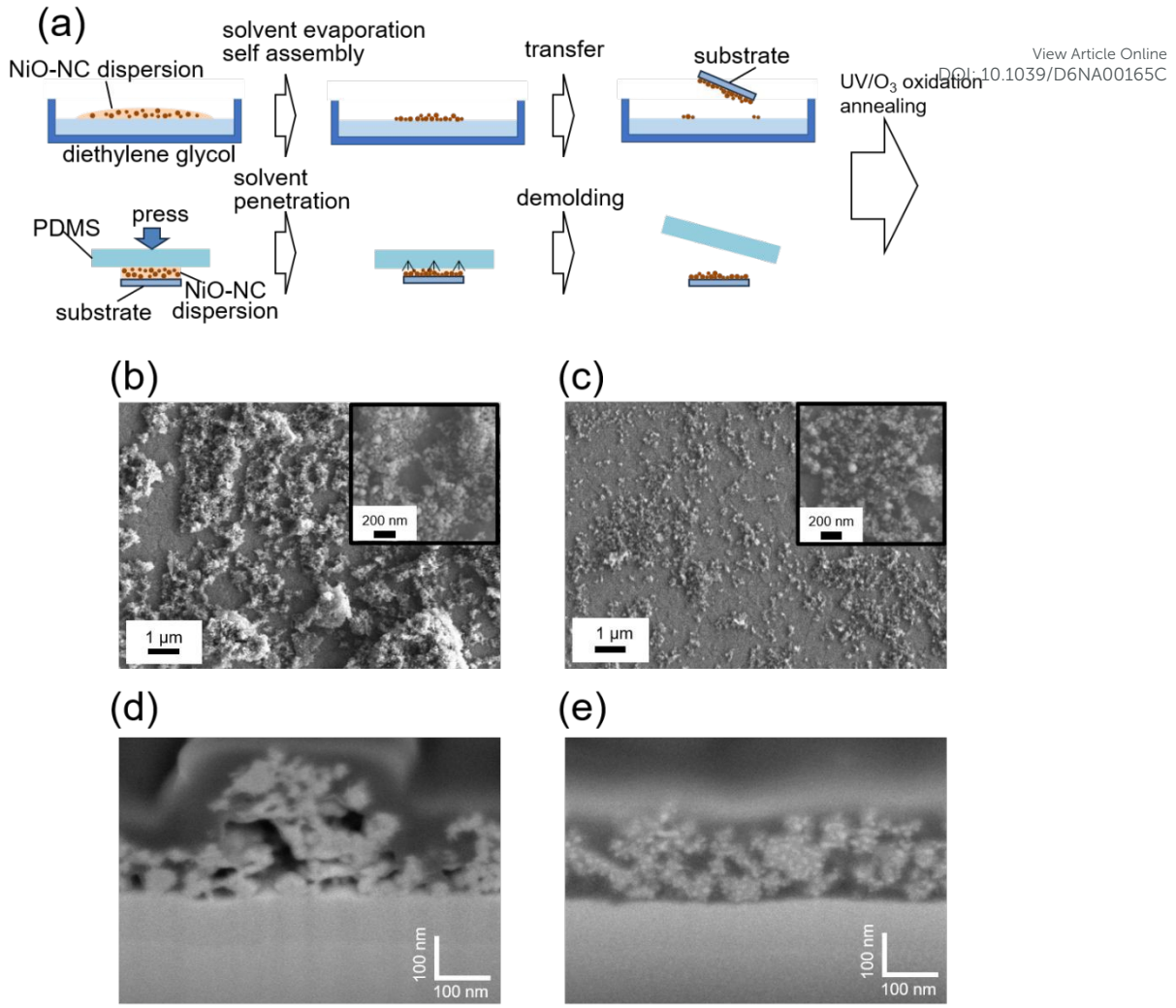

Fig. 2 (a) Fabrication of NiO-NC films: (upper) LS method, (lower) PC method. (b,c) FE-SEM images of the NiO-NC films prepared using (b) the LS method and (c) the PC method. Film preparation was performed from a 3 wt% NiO-NC dispersion in *n*-octane. The insets show magnified views of the SEM images. (d,e) Cross-sectional SEM images of the NiO-NC films (d) corresponding to the panel (b) and (e) corresponding to the panel (c).

Table 1. Parameters of the NiO-NC films prepared from a 3 wt% dispersion. R_a, $Rt_{\pm 50}$, and CR are the arithmetic mean roughness, thickness ratio in half interval, and coverage ratio, respectively

	thickness (nm) [a]	R_a (nm) [a]	$Rt_{\pm 50}$ [a]	CR (%) [b]
LS method	144	90	32	71
PC method	80	37	61	38

a: Evaluated by surface profiling.

b: Evaluated by FE-SEM.

film prepared using the PC method. Although the NiO-NC film prepared using the PC method appeared smooth over lateral distances of several hundred micrometers, its roughness was ~40 nm. This was attributed to the presence of local aggregates within the submillimeter range of the observation area, which increased the roughness value. To quantitatively compare the smooth regions of the NiO-NC films, the ratio of the region with a thickness within the average thickness ±50% ($Rt_{\pm 50}$) was calculated, as defined in Equation 1:

$$Rt_{\pm 50} = \frac{t_{\pm 50}}{t_{all}} \times 100 \quad (1)$$

where $t_{\pm 50}$ represents the region with a thickness within the average thickness ±50% and t_{all} is the region used to calculate the average thickness. The $Rt_{\pm 50}$ value of the NiO-NC film prepared using the PC method was approximately twice that of the film prepared using the LS method. Cross-sectional SEM images were examined to discuss the film morphology through the thickness direction (Figures 2d and 2e). The surface of the NiO-NC film prepared using the PC method was rough compared to that using LS-method as expected from the result of the top-view SEM image and height profiles. Furthermore, large interparticle voids with sizes ranging from several tens to hundreds of nanometers were observed. In contrast, although the NiO-NC films also include the interparticle voids with sizes less than 100 nm, the secondary particles were connected each other.

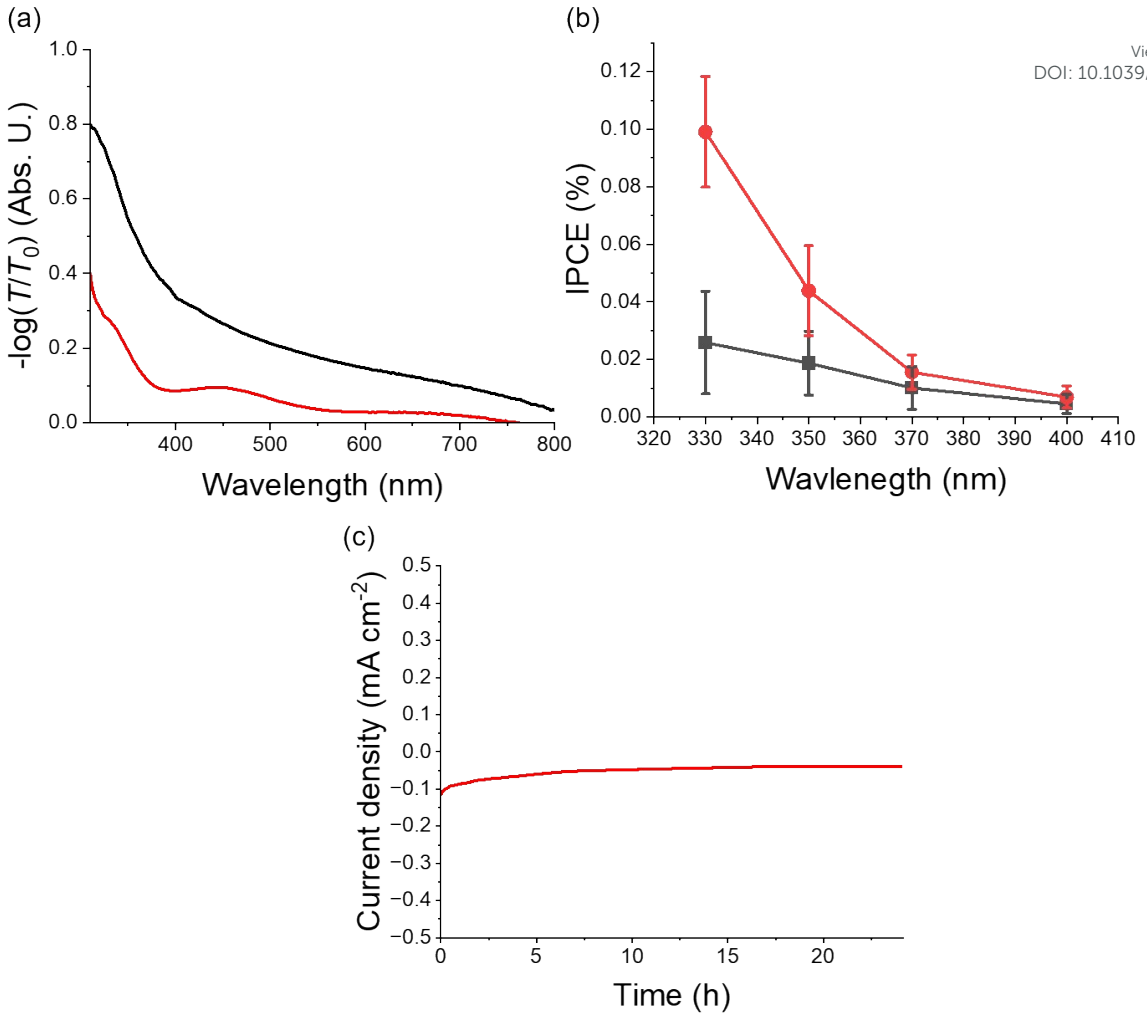

Fig. 3 (a) Extinction and (b) IPCE action spectra of NiO-NC films prepared using the (black) LS and (red) PC methods from a 3 wt% NiO-NC dispersion in *n*-octane. (c) Time dependence of the current value for NiO-NC films prepared using the PC method with the irradiation from the xenon lamp source.

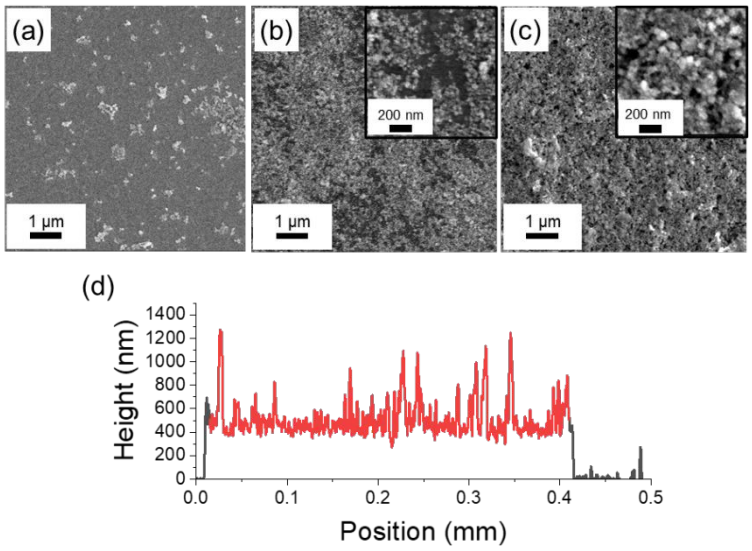

Fig. 4 FE-SEM images of NiO-NC films prepared using the PC method from dispersions of (a) 1 wt% NiO-NC and 10 wt% OA, (b) 5 wt% NiO-NC and 30 wt% OA, and (c) 10 wt% NiO-NC10 and 30 wt% OA. The insets in panels (b) and (c) show magnified views of the SEM images. (d) Height profile of the NiO-NC film prepared from dispersions of 10 wt% NiO-NC and 30 wt% OA.

Figure 3a shows the extinction spectra of the NiO-NC films on TEC glass. The NiO-NC films prepared using both the PC and LS methods exhibited strong absorption at wavelengths below 380 nm, corresponding to NiO excitation. The NiO-NC film prepared using the LS method displayed higher extinction across the observed wavelength range, likely due to increased scattering from aggregates. The energy band gap of the NiO-NC film prepared using the PC method, as determined from the Tauc plot, was 3.5 eV (Figure S3).[48]

To evaluate the reduction ability of the NiO-NC film photocathodes, the incident photon-to-current efficiency (IPCE) was measured using a conventional three-electrode electrochemical setup under UV photoirradiation (Figure 3b). Cathodic currents were observed for the photocathodes of both films, indicating that the electrons generated through NiO excitation participated in the reduction reactions, whereas the holes migrated through the NiO film to the counter electrode. At 330 nm, the IPCE of the NiO-NC film prepared using the PC method was ~3-times higher than that of the film prepared using the LS method. This was attributed to the fact that the large aggregates of NiO-NCs in the film prepared using the LS method contain large interparticle voids, which hinder hole transfer.[23, 49] In contrast, the interconnections between secondary particles of NiO NCs in the film prepared using the PC method support hole migration. Additionally, the NiO-NC film photocathodes prepared using the PC method showed stable current for at least 24 h, with an average current density of 51 μA cm^{-2} and a standard deviation of 15 μA cm^{-2}, as shown in Figure 3c.

Overall, the NiO-NC film prepared using the PC method exhibited a smoother surface and higher charge separation ability than the film prepared using the LS method. However, the CR of the NiO-NCs on the substrate remained below 40%, as some NiO NCs adhered to the PDMS mold surface (Figure S4a). It was therefore speculated that the additional OA acts as a release reagent because the coexistence of aliphatic acids renders the surface of the molded mixture hydrophobic.[50] Photographic images of the substrate and mold after film fabrication showed that the residual NiO-NCs on the mold decreased with increasing OA content (Figures S4b and S4c).

Thickness dependence and hole migration mechanism in NiO-NC films

Thickness plays a key role in determining the optical, electrical, and electronic properties of semiconductor cathodes, and the homogeneity of these properties in the thickness direction is crucial for designing optoelectronic devices. The photoelectrochemical performance of NiO-NC films prepared using the PC method was evaluated for varying film thicknesses, which were controlled by adjusting the NiO-NC and OA concentrations in the dispersion. Figures 4a–4c show the FE-SEM images of the corresponding NiO-NC films, demonstrating that CR increased with NiO-NC concentration, reaching 95% for NiO-NC and OA concentrations of 10 and 30 wt%, respectively. The height profiles of these films, prepared at the same concentrations, are presented in Figure 4d, revealing a thickness and $Rt_{\pm 50}$ of ~500 nm and 73%, respectively. This indicates that a smooth surface was maintained in the NiO-NC film at this thickness. Table 2 summarizes the thickness, surface roughness, $Rt_{\pm 50}$, and CR of the NiO-NC films prepared under various conditions. The film thickness increased with NiO-NC concentration, while the CR was enhanced in the presence of OA and increased gradually with increasing NiO-NC concentration.

These results raise the question of how variations in film preparation conditions influence hole migration. Figure 5a shows the IPCE and CR as functions of NiO-NC film thickness. The CR increased with increasing thickness, whereas the IPCE did not exhibit a clear thickness dependence. To evaluate the photocathode performance of the deposited regions of the NiO-NC films, the IPCE values were normalized by the CR to yield the normalized IPCE (NIPCE), as expressed in Equation 2:

$$\mathrm{NIPCE} = \frac{\mathrm{IPCE}}{\mathrm{CR}} \times 100 \qquad (2)$$

The NIPCE, which is overlaid in Figure 5a, was found to be inversely proportional to film thickness. This observation suggests that NiO-NC films prepared using the PC method can be represented as homogeneous series impedances that are independent of the NiO-NC and OA concentrations. Figure 5a includes duplicate samples prepared from dispersions containing 10 wt% NiO NC and 10 wt% OA (open circles) and those containing 10 wt% NiO NC and 30 wt% OA (filled circles). Although their thicknesses and CR values fluctuate, the NIPCE values follow an inverse relationship with film thickness.

For comparison, a photocathode system with properties controlled by a parameter independent from film thickness was considered. Our group previously reported that plasma-enhanced (PE)-ALD, which produces compact oxide layers via a self-limiting, layer-by-layer growth mechanism using gas-phase precursors, enables the filling of interparticle voids in NiO films and establishes continuous hole migration pathways.[23] Because the NiO layer deposited by ALD is electrochemically distinct from the pre-existing NiO-NC matrix, the PC/ALD film was treated as a useful inhomogeneous control system against the electrochemically homogeneous NiO-NC film. The ALD method was then applied to NiO-NC films prepared from a 3 wt% NiO-NC dispersion using the PC method (PC/ALD method). Figure 5b shows the IPCE and NIPCE values as a function of the number of ALD cycles. The IPCE values increased markedly with increasing ALD cycles, while the bulk film thickness showed only minimal changes. This indicates that filling the interparticle voids facilitated hole migration. Furthermore, the photoelectrochemical performance of these NiO films including NiO-NC and NiO deposited by the ALD did not exhibit a clear dependence on film thickness.

The difference in charge separation behavior between the NiO-NC films prepared using the PC and PC/ALD methods is evident from the electrochemical impedance spectra (EIS, Figure S5). The Nyquist plot of the NiO-NC film prepared using the PC method was analyzed using an equivalent circuit comprising two impedance layers connected in series, namely the interfacial charge-transfer layer and the bulk charge transport layer (Figure 5c).[51] In contrast, the EIS of the NiO-NC film prepared using the PC/ALD method indicates the presence

View Article Online
DOI: 10.1039/D6NA00165C

Table 2. Parameters of the NiO-NC films prepared using the PC method from dispersions with varying concentrations of NiO-NC and OA

NiO-NC concentration (wt%)	OA concentration (wt%)	thickness (nm) [a]	R_a (nm) [a]	$Rt_{\pm 50}$ [a]	CR (%) [b]
1	10	30	22	21	4
1	30	45	29	43	13
3	10	130	47	61	85
3	30	108	58	43	86
5	10	192	62	59	87
5	30	166	114	36	88
10	10	226	81	57	98
10	30	518	114	73	95

a: Evaluated by surface profiling.

b: Evaluated by FE-SEM.

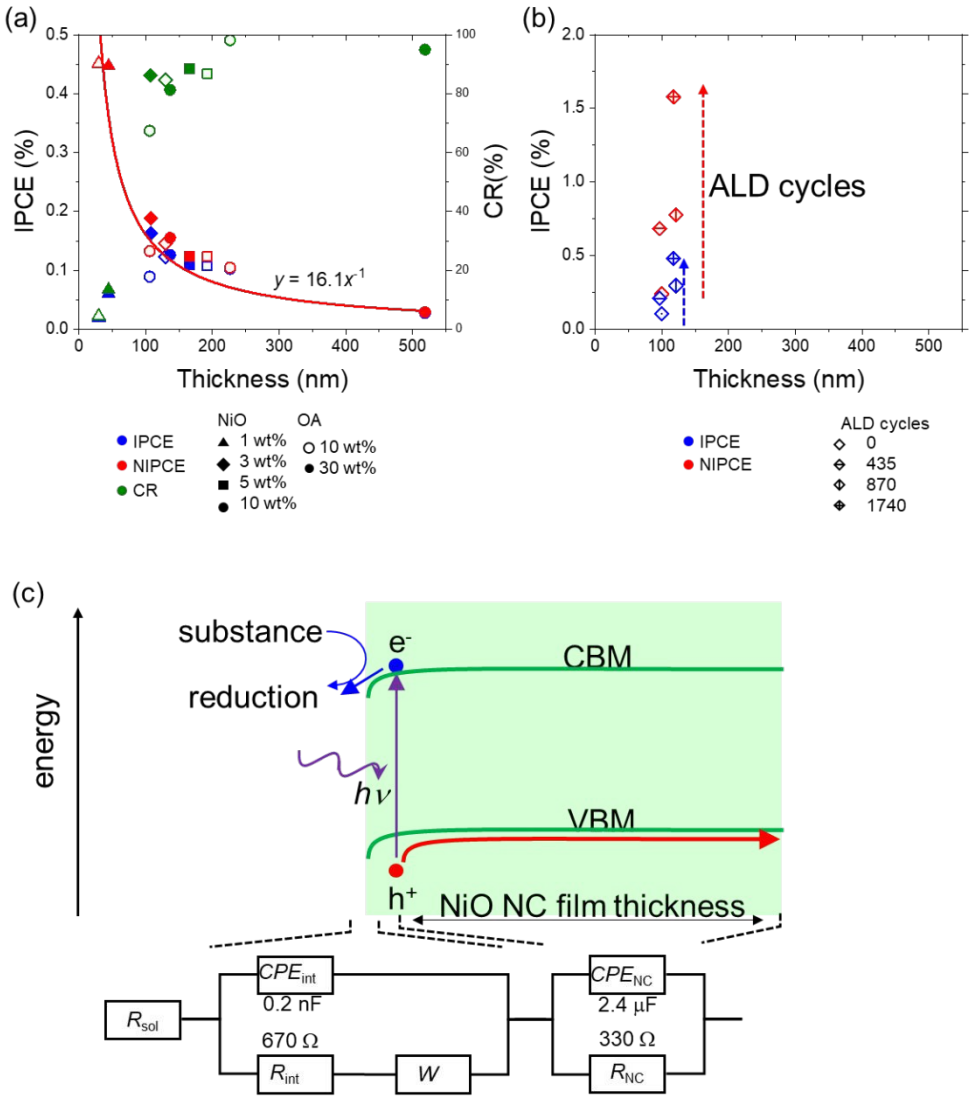

Figure 5. (a) Thickness dependences of IPCE, NIPCE, and CR for the NiO-NC films prepared using varying concentrations of NiO-NC and OA. (b) Thickness dependences of IPCE, NIPCE, and CR for the NiO-NC films prepared using a 3 wt% NiO-NC dispersion after additional deposition of NiO by PE-ALD. Arrows are shown for clarity of the increment of ALD cycle. IPCE and NIPCE were obtained at 330 nm. (c) Energy diagram of the semiconductor/electrolyte interface with the corresponding electrical circuit analog. R_{sol}, R_{int}, and R_{NC} are the resistances in solution, at the solution–substrate interface, and of the bulk NiO-NC film, respectively. CPE_{int} and CPE_{NC} are the constant phase elements for the solution–substrate interface and the bulk NiO-NC film, respectively. W is the Warburg diffusion impedance.

of an additional impedance component derived from the ALD-NiO layer formed between the NiO-NCs.

Overall, NiO-NC films with thicknesses ranging from ~100 to 500 nm were successfully fabricated using the PC method by

varying the concentrations of NiO NCs and OA in the dispersions. Importantly, films fabricated under these conditions can be regarded as photoelectrochemically homogeneous photocathodes, whose series impedances are proportional to film thickness (Figure 5c).

Conclusions

NiO NCs with high crystallinity, small particle size, and a narrow size distribution were synthesized via supercritical hydrothermal synthesis. Simultaneously, *in-situ* OA modification of the NiO NC surfaces was achieved during synthesis. Dispersions of NiO NCs in *n*-octane were employed for film fabrication using the PC method. Compact NiO-NC films with relatively low roughness were produced, compared with those obtained using the LS method. Furthermore, NiO-NC films with thicknesses ranging from ~100 to 500 nm were prepared using the PC method by varying the concentrations of NiO-NC and OA in the precursor dispersions. These films functioned as photocathodes and can be regarded as photoelectrochemically homogeneous photocathodes with series impedances proportional to thickness. Film thickness was identified as an important parameter for controlling optical resonance, optical path length, and device size in optoelectronic applications. Consequently, photoelectrochemical homogeneity enhances the design flexibility of NiO photocathode devices. Moreover, compact packing of NiO-NCs reduced the number of interparticle voids, enhancing hole migration and charge separation efficiency while also suppressing surface roughness and tuning the refractive index of the NiO layers. To achieve this, it is necessary to narrow the size distribution and enhance dispersibility by optimizing the supercritical synthesis conditions, which can be performed through appropriate selection of the modifier and solvent species. Well-dispersed NiO NCs are expected to improve reproducibility of the film. Furthermore, connection between nanoparticles in nanoscale remains a challenge. A novel method is desired to achieve interparticle filling with high throughput such as additional deposition of NiO layer by sol-gel process using dilute precursor solution[23] or chemical sintering.[52] From the perspective of semiconductor engineering, carrier doping via incorporation of dopant compounds during supercritical synthesis allows control of the carrier density and band energy of NiO NCs. The combination of supercritical synthesis of p-type semiconductor NCs with compact film formation via the PC method offers a green and economically advantageous approach, minimizing material loss and reducing the use of hazardous organic solvents. These findings demonstrate the potential of combining supercritical synthesis and PC methods for the high-throughput manufacturing of NiO photocathodes.

Materials and Methods

Synthesis of NiO NCs under super critical hydrothermal conditions

A 0.1 mol dm^{-3} nickel oxide precursor solution was prepared by dissolving nickel nitrate hexahydrate in purified water. An aliquot of this solution (5 mL) was transferred to a pressure-resistant vessel (inner volume of 10 mL) with OA (1.5 mmol). The hydrothermal reaction was performed at 400°C for 20 min in an electric furnace (SAH-R16-500, AKICO) with shaking. Using the NIST Chemistry WebBook,[53] the internal pressure during the reaction was estimated to be 38 MPa. The reaction was terminated by submerging the reactor in a water bath at room temperature. The NiO NCs were subjected to centrifugation several times in the presence of additional ethanol and dried in a vacuum oven to yield the powdered NiO NCs.

A dispersion of NiO NCs in *n*-octane was prepared by performing a supercritical reaction under the above conditions with the addition of *n*-octane (0.5 mL). After the reaction, the organic phase, which contained the NiO-NCs, was collected and the NiO-NCs were washed by centrifugation using additional *n*-octane. The NiO-NC and OA concentrations in the dispersion were adjusted by the addition of *n*-octane and OA, respectively.

Fabrication of the NiO-NC films

The NiO-NC films were prepared on TEC glass (1052, Geomatic, 10 × 10 × 0.7 mm^3) according to the LS and PC methods. Specifically, for the LC method, a NiO-NC layer was formed by dropping an aliquot (5 µL) of the NiO-NC dispersion in *n*-octane onto the diethylene glycol surface and drying to remove the *n*-octane. Subsequently, the NiO-NC layer was transferred onto the TEC glass surface, and the substrate was annealed for 1 h at 80 °C to remove diethylene glycol. For the PC method, an aliquot (5 µL) of the NiO-NC dispersion in *n*-octane was dropped onto a TEC glass substrate and compressed overnight using a PDMS sheet on a SiO_2 support. Pressure was applied using the dead weight of a tablet molding machine (E863, JASCO). Both NiO-NC films were subjected to UV/O_3 treatment (PL16-110, Sen-Lights) for 10 min and annealed at 600°C for 2 h.

For the PE-ALD process, NiO was deposited at 300 °C using a PE-ALD reactor (AD-230LP-H, Samco). Bis(cyclopentadienyl) nickel ($Ni(CP)_2$) was used as the Ni precursor, maintained at 100 °C. Consequently, gaseous $Ni(CP)_2$ was transported to the reaction chamber by N_2 carrier gas at a flow rate of 100 sccm. O_2 plasma was generated using a radio frequency power of 150 W and an O_2 flow rate of 100 sccm. Each deposition cycle consisted of a 0.05 s $Ni(CP)_2$ pulse, 2 s N_2 purging, 3 s O_2-plasma pulse, and 2 s N_2 purging. The deposition rate of NiO on the flat TEC glass was 0.017 nm/cycle.

Optical spectral measurements

Transmission spectra were recorded at room temperature using a UV/Vis spectrometer (Lambda 265, Perkin Elmer). A TEC glass substrate was used as a reference. FTIR spectra were recorded at room temperature using an FTIR spectrometer (FT/IR-4200, JASCO) using KBr as the matrix for the NiO-NC powders.

Material characterization

The morphology and size of the NiO NCs were analyzed using TEM (JEM-2100Plus, JEOL) at 120 kV. For this purpose, the TEM samples were prepared by transferring the NiO NCs onto carbon-coated copper grids (COL-C10; Okenshoji). The crystallinity and crystal orientation of the NiO NCs were analyzed using XRD (CuKα, SmartLab3G, Rigaku). The surface morphology of the NiO-NC film and the CR of the TEC glass substrate bearing NiO NCs were examined using FE-SEM (S-

View Article Online
DOI: 10.1039/D5NA00165C

4800, Hitachi) at 5 kV. The cross-sectional SEM images were obtained using FIB-SEM (Helios 600i Dual Beam, Thermo Fisher Scientific). The carbon layer with a thickness of several hundreds of nanometers was deposited on the NiO-NC films by electron beams, then the cross section was exposed by FIB milling of Ga ions with an acceleration voltage of 30 kV. The exposed cross-sections were observed with an acceleration voltage of 2 kV at a tilt angle of 52°.

The thickness and roughness of the NiO-NC film were evaluated from the height profiles obtained using a surface profiler (ET4000A, Kosaka Laboratory).

Photoelectrochemical reaction

Ag paste was applied to the conductive layer of the substrate and connected to an electrochemical analyzer (ALS/CH Instruments 612E, ALS) using a copper wire. An aqueous solution of Na_2SO_4 (0.1 mol dm^{-3}) was used as the supporting electrolyte. An 800 W xenon lamp was employed as the light source. For the IPCE measurements, a standard three-electrode system was employed using a platinum wire as the counter electrode and an Ag/AgCl electrode as the reference electrode. The working electrode potential was set to −1.0 V vs. Ag/AgCl to obtain the current–time characteristics of the NiO-NC films on TEC glass. Bandpass filters with bandwidths of <15 nm were employed. EIS measurements were conducted using the same setup as that employed for the IPCE measurements. Nyquist plots were recorded in the frequency range of 1 Hz–1 MHz, and the results were analyzed using PyZwx software.[54]

Author contributions

Tomoya Oshikiri: Conceptualization, Resources, Data curation, Funding acquisition, Validation, Visualization, Methodology, Writing – original draft, Project administration, Investigation, Tomoki Kawase: Data curation, Investigation, Visualization, Writing – original draft, Kaori Sato: Investigation, Hazuki Ito: Investigation, Takaaki Tomai: Resources, Data curation, Methodology, Writing – review & editing, Keisuke Nakamura: Investigation, Xu Shi: Investigation, Yasutaka Matsuo: Investigation, Hiromasa Niinomi: Data curation, Writing – review & editing, Masaru Nakagawa: Conceptualization , Supervision, Project administration, Writing – review & editing, Funding acquisition, Resources

Conflicts of interest

There are no conflicts of interest to declare.

Data availability

The data that support the findings of this study are available from the corresponding author upon reasonable request.

Acknowledgements

This work was supported by JSPS KAKENHI Grant Numbers JP25K22238, JP25H00828, JP23K23113, JP23H01916, JP23K04902, JP22H05136, JP22H05131 (Grant-in-Aid for Transformative Research Areas “Evolution of Chiral Materials Science using Helical Light Fields”), and the “Crossover Alliance to Create the Future with People, Intelligence and Materials” from MEXT, Japan. This work also utilized the “Advanced Research Infrastructure for Materials and Nanotechnology in Japan (ARIM)” of MEXT (Proposal Numbers JPMXP1224HK0039 and JPMXP1224TU0018), and from the GIMRT Program of the Institute for Materials Research (Proposal No. 322H051360), Tohoku University, Material Solutions Center (MaSC), Central Analytical Facility (CAF), Tohoku University.

Notes and references

1. N. A. M. Barakat, M. S. Khil, F. A. Sheikh and H. Y. Kim, *J. Phys. Chem. C*, 2008, **112**, 12225-12233.
2. A. Visibile, R. B. Wang, A. Vertova, S. Rondinini, A. Minguzzi, E. Ahlberg and M. Busch, *Chem. Mater.*, 2019, **31**, 4787-4792.
3. K. Schneider, *J. Mater. Sci.: Mater.*, 2020, **31**, 10478-10488.
4. R. C. Sharma, R. Nandal, N. Tanwar, R. Yadav, J. Bhardwaj and A. Verma, *J. Phys.: Conf. Ser.*, 2023, **2426**, 012008.
5. J.-W. Liang, Y. Firdaus, C. H. Kang, J.-W. Min, J.-H. Min, R. H. Al Ibrahim, N. Wehbe, M. N. Hedhili, D. Kaltsas, L. Tsetseris, S. Lopatin, S. Zheng, T. K. Ng, T. D. Anthopoulos and B. S. Ooi, *ACS Appl. Mater. Interfaces*, 2022, **14**, 17889-17898.
6. H. Sato, T. Minami, S. Takata and T. Yamada, *Thin Solid Films*, 1993, **236**, 27-31.
7. H. Nakai, M. Sugiyama and S. F. Chichibu, *Appl. Phys. Lett.*, 2017, **110**, 181102.
8. H. Ohta, M. Hirano, K. Nakahara, H. Maruta, T. Tanabe, M. Kamiya, T. Kamiya and H. Hosono, *Appl. Phys. Lett.*, 2003, **83**, 1029-1031.
9. K. Nakamura, T. Oshikiri, K. Ueno, Y. Wang, Y. Kamata, Y. Kotake and H. Misawa, *J. Phys. Chem. Lett.*, 2016, **7**, 1004-1009.
10. H. H. Abdelhalium, M. S. Abdel-Wahab, M. T. Tamm and W. Z. Tawfik, *Appl. Phys. A*, 2023, **129**.
11. X. Cui, X. Zhang, T. Guo, G. Tang, J. Jin, Z. Zhu, D. Chu, Y. Gou, J. Li, Y. Guo, J. Robertson and Q. Tai, *Adv. Func. Mater.*, 2025, **35**.
12. N. M. El-Shafai, M. Abdelfatah, I. M. El-Mehasseb, M. S. Ramadan, M. M. Ibrahim, A. El-Shaer, M. A. El-Kemary and M. S. Masoud, *Sep. Purif. Technol*, 2021, **267**, 118631.
13. I. Hotovy, J. Huran, P. Siciliano, S. Capone, L. Spiess and V. Rehacek, *Sens. Actuators B: Chem.*, 2001, **78**, 126-132.
14. N. V. Srinivasa, K. Haunsbhavi, N. Srinatha, H. M. Mahesh, S. Valanarasu and B. Angadi, *Mater. Sci. Eng. B*, 2024, **301**, 117178.
15. Y. Ding, X. Guo, Y. Zhou, Y. He and Z. Zang, *J. Mater. Chem. C*, 2022, **10**, 16218-16246.
16. H. Robatjazi, S. M. Bahauddin, C. Doiron and I. Thomann, *Nano Lett.*, 2015, **15**, 6155-6161.
17. R. Kamata, H. Kumagai, Y. Yamazaki, G. Sahara and O. Ishitani, *ACS Appl. Mater. Interfaces*, 2019, **11**, 5632-5641.
18. J. S. Duchene, G. Tagliabue, A. J. Welch, X. Li, W.-H. Cheng and H. A. Atwater, *Nano Lett.*, 2020, **20**, 2348-2358.
19. J. Wu, M. Meng, X.-D. Du, M. Li, L. Jin and W. Liu, *Inorganic Chemistry*, 2024, **63**, 6192-6201.
20. Y. Zheng, E. Wang, J. Zhou and Z. Sun, *ACS Mater. Lett.*, 2024, **6**, 3572-3601.
21. T. Jia, M. Ruan, G. Li, P. Michorczyk, C. Wang and Z. Liu, *J. Mater. Chem. A*, 2026, **14**, 1908-1922.
22. C. Yan, M. Ruan, C. Wang, T. Zhong, M. Zhou, L. Zhou and Z. Liu, *Nano Energy*, 2026, **151**, 111852.

View Article Online
DOI: 10.1039/D6NA00165C

23. T. Oshikiri, T. Katsurahara, N. Kubota, T. Tezuka, K. Araki, X. Shi, Y. Matsuo, H. Niinomi, H. Misawa and M. Nakagawa, *Chem. Eur. J.*, 2025, **31**, e202501332.
24. A. Agrawal, H. R. Habibi, R. K. Agrawal, J. P. Cronin, D. M. Roberts, R. Caronpopowich and C. M. Lampert, *Thin Solid Films*, 1992, **221**, 239-253.
25. I. Hotovy, J. Liday, L. Spiess, H. Sitter and P. Vogrincic, *Jpn. J. Appl. Phys.*, 2003, **42**, L1178-L1181.
26. D. Koushik, M. Jošt, A. Dučinskas, C. Burgess, V. Zardetto, C. Weijtens, M. A. Verheijen, W. M. M. Kessels, S. Albrecht and M. Creatore, *J. Mater. Chem. C*, 2019, **7**, 12532-12543.
27. K. Nakamura, T. Oshikiri, K. Ueno, T. Katase, H. Ohta and H. Misawa, *J. Phys. Chem. C*, 2018, **122**, 14064-14071.
28. T. Oshikiri, H. Sawayanagi, K. Nakamura, K. Ueno, T. Katase, H. Ohta and H. Misawa, *J. Chem. Phys.*, 2020, **152**, 034705.
29. T. Oshikiri, H. Jo, X. Shi and H. Misawa, *Chem. Eur. J.*, 2022, **28**, e202200288.
30. L. Qiao and M. T. Swihart, *Adv. Colloid Interface Sci.*, 2017, **244**, 199-266.
31. D. A. Brewster, Y. Bian and K. E. Knowles, *Chem. Mater.*, 2020, **32**, 2004-2013.
32. T. Kimijima, K. Kanie, M. Nakaya and A. Muramatsu, *Appl. Cat. B: Environ.*, 2014, **144**, 462-467.
33. M. Salavati-Niasari, N. Mir and F. Davar, *Polyhedron*, 2009, **28**, 1111-1114.
34. D. C. Onwudiwe, N. H. Seheri, L. Hlungwani, H. Ferjani and R. Rikhotso-Mbungela, *J. Mol. Struct.*, 2024, **1317**, 139084.
35. J. Zhang, S. Ohara, M. Umetsu, T. Naka, Y. Hatakeyama and T. Adschiri, *Adv. Mater.*, 2007, **19**, 203-206.
36. A. Yoko, G. Seong, T. Tomai and T. Adschiri, *KONA Powder Part. J.*, 2020, **37**, 28-41.
37. A. Yoko, Y. Tanaka, G. Seong, D. Hojo, T. Tomai and T. Adschiri, *J. Phys. Chem. C*, 2020, **124**, 4772-4780.
38. T. Adschiri, Y.-W. Lee, M. Goto and S. Takami, *Green Chem.*, 2011, **13**, 1380.
39. I. Marica, M. Stefan, S. Boca, A. Falamaş and C. Farcău, *J. Colloid Interface Sci.*, 2023, **635**, 117-127.
40. Y. Zhao and J. S. Marshall, *Phys. Fluids*, 2008, **20**, 043302.
41. M. S. Kim, L. Ma, S. Choudhury, S. S. Moganty, S. Wei and L. A. Archer, *J. Mater. Chem. A*, 2016, **4**, 14709-14719.
42. M. Swierczewski and T. Bürgi, *Langmuir*, 2023, **39**, 2135-2151.
43. M. Ikawa, T. Yamada, H. Matsui, H. Minemawari, J. Y. Tsutsumi, Y. Horii, M. Chikamatsu, R. Azumi, R. Kumai and T. Hasegawa, *Nat. Commun.*, 2012, **3**, 1176.
44. V. Vohra, W. Mróz, S. Inaba, W. Porzio, U. Giovanella and F. Galeotti, *ACS Appl. Mater. Interfaces*, 2017, **9**, 25434-25444.
45. S. Inaba, R. Arai, G. Mihai, O. Lazar, C. Moise, M. Enachescu, Y. Takeoka and V. Vohra, *ACS Appl. Mater. Interfaces*, 2019, **11**, 10785-10793.
46. R. Lenin and P. A. Joy, *J. Colloid Interface Sci.*, 2017, **506**, 162-168.
47. J. Ibarra, J. Melendres, M. Almada, M. G. Burboa, P. Taboada, J. Juárez and M. A. Valdez, *Mater. Res. Exp.*, 2015, **2**, 095010.
48. M. Hashem, E. Saion, N. M. Al-Hada, H. M. Kamari, A. H. Shaari, Z. A. Talib, S. B. Paiman and M. A. Kamarudeen, *Results Phys.*, 2016, **6**, 1024-1030.
49. S. Liu, R. Liu, Y. Chen, S. Ho, J. H. Kim and F. So, *Chem. Mater.*, 2014, **26**, 4528-4534.
50. T. A. Saleh, N. Baig, H. A. Othman and A. M. Al Harith, *Chem. Eng. J.*, 2021, **407**, 126216.
51. T. Lopes, L. Andrade, F. Le Formal, M. Gratzel, K. Sivula and A. Mendes, *Phys. Chem. Chem. Phys.*, 2014, **16**, 16515.
52. N. G. Park, K. M. Kim, M. G. Kang, K. S. Ryu, S. H. Chang and Y. J. Shin, *Adv. Mater.*, 2005, **17**, 2349-2353.
53. NIST Chemistry WebBook, SRD 69, https://webbook.nist.gov/chemistry, (accessed October, 2024).
54. K. Kobayashi and T. S. Suzuki, *Electrochem.*, 2021, **89**, 218-222.

View Article Online
DOI: 10.1039/D6NA00165C

Data availability

The data that support the findings of this study are available from the corresponding author upon reasonable request.